JASA ARTICLE

Effects of acoustic nonlinearity on pulse-echo attenuation coefficient estimation from tissue-mimicking phantoms

Andres Coila[a] and Michael L. Oelze
Beckman Institute of Advanced Science and Technology, Department of Electrical and Computer Engineering, University of Illinois at Urbana-Champaign, Urbana, Illinois 61801, USA

ABSTRACT:
The ultrasonic attenuation coefficient (ACE) can be used to classify tissue state. Pulse-echo spectral-based attenuation estimation techniques, such as the spectral-log-difference method (SLD), account for beam diffraction effects using a reference phantom having a sound speed close to the sound speed of the sample. Methods like SLD assume linear propagation of ultrasound and do not account for potential acoustic nonlinear distortion of the backscattered power spectra in both sample and reference. In this study, the ACE of a sample was computed and compared using the SLD with two independent references (high attenuating and low attenuating phantoms but with similar B/A values) and over several pressure levels. Both numerical and physical tissue-mimicking phantoms were used in the study. The results indicated that the biases in ACE increased when using a reference having low attenuation, whereas the high attenuating reference produced more consistent ACE. Furthermore, increments in ACE vs input pressure were correlated to the log-ratio of Gol'dberg numbers between the sample and reference ($R^2 = 0.979$ in simulations and $R^2 = 0.734$ in experiments). Therefore, the results suggest that to reduce bias in ACE using spectral-based methods, both the sound speed and the Gol'dberg number of the reference phantom should be matched to the sample.
 https://doi.org/10.1121/10.0001690
(Received 23 January 2020; revised 16 July 2020; accepted 17 July 2020; published online 17 August 2020)
[Editor: Charles C. Church] Pages: 805–814

I. INTRODUCTION

The attenuation coefficient is an acoustical property of tissues and has been used as a quantitative ultrasonic parameter for tissue characterization, including recent studies in liver (Jeon *et al.*, 2019), breast (Nasief *et al.*, 2019), placenta (Deeba *et al.*, 2019), or indirectly in muscle (Weng *et al.*, 2019), among other biological tissues. Empirical results from studies have found that the attenuation coefficient, $\alpha(f)$, for several soft tissues follows a power-law function vs frequency f, i.e., $\alpha(f) = \alpha_0 f^{\gamma}$, where α_0 is an attenuation coefficient factor and γ is the frequency dependent exponent, commonly $\gamma \in (1, 2)$ (Cobbold, 2017, p. 74). Hence, current methods for estimating attenuation coefficients are performed mainly in the frequency domain. Moreover, spectral-based methods in pulse-echo mode for attenuation estimation *in vivo* using backscattered signals assume that the power spectrum of a region of interest is proportional to the product of the system acquisition effects (scanner, transducer, and diffraction) along with effects derived from intrinsic acoustic properties of the medium (cumulative attenuation and backscatter coefficient) (Labyed and Bigelow, 2011; Mamou and Oelze, 2013). Furthermore, as found by Fatemi and Greenleaf (1996), in pulse-echo experiments, the envelope of backscattered signals from a region of interest is susceptible to changes in the input pressure levels. For example, an increment of the peak pressure as low as 9 dB could generate strong distortion of the echo envelope measured from a wire target. Such distortions in the echo envelope manifest as excess attenuation at the larger input pressure levels, i.e., an estimated attenuation of the medium can be dependent on the input pressure level. This phenomenon occurs due to the inherent acoustic nonlinear propagation in the propagation path between the transducer and the targeted region. However, to the authors' knowledge, no study has been conducted to quantify how nonlinear distortion affects the estimation of attenuation when using pulse-echo spectral-based methods.

In a fluid nonlinear medium, the degree of nonlinearity is typically characterized by its nonlinearity parameter B/A, where A and B are the first and second order terms in the isentropic power series expansion of the total pressure P (equilibrium pressure P_0 plus acoustic pressure p) as function of density ρ, namely, the adiabatic equation of state

$$P = P_0 + \left.\frac{\partial P}{\partial \rho}\right|_{\rho=\rho_0} (\rho - \rho_0) + \left.\frac{\partial^2 P}{\partial \rho^2}\right|_{\rho=\rho_0} (\rho - \rho_0)^2 + \cdots, \tag{1}$$

where ρ_0 is the equilibrium density, $A \equiv (\partial P/\partial \rho)|_{\rho=\rho_0}$ and $B \equiv (\partial^2 P/\partial \rho^2)|_{\rho=\rho_0}$. Whereas truncation of the Eq. (1) up to the first order provides the linear acoustic wave equation, truncation up to the second order term can later be combined with the equation of momentum and equation of continuity of fluids (also truncated up to the second order) to obtain nonlinear expressions for the acoustic pressure (Pierce,

[a]Electronic mail: acoila@illinois.edu, ORCID: 0000-0002-2924-3888.

1989, Chap. 11) of a propagating mono-frequency acoustic plane wave. An important result of this treatment is that sound speed has a dependence of the acoustic pressure and distortion of the propagating wave further results in generation of the second, third, and higher order harmonics. These harmonics require that energy be transferred out of the fundamental frequency. Moreover, other effects such as shock waves and saturation can be observed. Hence, when using ultrasound for imaging tasks, such as medical diagnostics, it cannot be assumed that these nonlinear phenomena will be absent. Because backscattering from soft tissues is small compared to the incident field, in order to improve the signal-to-noise ratio for specific imaging tasks, larger input pressure levels (excitation levels, energy levels, etc.) are often used during data acquisition resulting in a higher likelihood of nonlinear distortion of the ultrasound.

A descriptive parameter for nonlinearity, called the Gol'dberg number, provides a rule of thumb to predict the degree of acoustic nonlinearity anticipated during the transmission of a plane wave with frequency f_0 in a lossy media. The Gol'dberg number is computed as $\Gamma = \beta kM/\alpha(f_0)$ (Kinsler *et al.*, 2000), where k is the wave number, $\beta \equiv 1 + [(1/2)B/A]$, is the nonlinearity coefficient of the medium, M is the Mach-number equal to the particle velocity amplitude at the source divided by the equilibrium sound speed of the medium, and $\alpha(f_0)$ is the attenuation coefficient of the medium. $\Gamma \ll 1$ predicts the acoustic nonlinearity to be negligible, whereas $\Gamma \gg 1$ predicts significant nonlinearitiy can be expected to develop. Moreover, a large Gol'dberg number implies that a non-negligible generation of harmonics ($2f_0$, $3f_0$, etc.) and energy transferred out of the fundamental frequency f_0 occurs at short propagation distances. Similar behavior (generation of harmonics) could be expected for a broadband pulse wave propagation where there is a band of frequencies propagating rather than a mono-frequency wave, in which case a second and third harmonic bands are generated out of energy from the fundamental frequency band.

Most pulse-echo based attenuation estimation methods use the power spectra of the fundamental frequency band. In a previous study, we demonstrated that the presence of nonlinear distortion adversely affects estimates of the backscatter coefficient changing both the slope and magnitude of the backscatter coefficient spectrum (Coila and Oelze, 2019). The slope of the backscatter coefficient is affected by nonlinearity because the strength of the nonlinear distortion is higher with higher frequency. Therefore, we aim to quantify how much the harmonic generation might also lead to inaccuracies in attenuation coefficient estimation when using a spectral-based estimation method, especially when large acoustic pressures are used. In the present work we analyzed a representative method for attenuation coefficient estimation in the frequency domain, namely, the spectral log difference (SLD) method for estimating the attenuation coefficient. In this paper, analysis of attenuation coefficient estimation inaccuracy in the presence of nonlinear media will first be performed in numerical simulations using the k-Wave toolbox (Treeby *et al.*, 2012) and then corroborated with experiments in physical phantoms. The acoustic pressure amplitudes used in this work were within the Food and Drug Administration (FDA) regulated limits for diagnostic ultrasound determined by the mechanical index ($\text{MI} \equiv \text{PNP}/\sqrt{f_0} < 1.9$), where PNP is the peak negative pressure (after derating by a factor of 0.3 dB/cm/MHz when measured in water).

II. METHODS

A. Spectral log difference

Assuming linear acoustic propagation, the power spectra of two gated windows (proximal and distal relative to the transducer surface) in a sample can be written as

$$S(f,z_p) = P(f)D(f,z_p)\sigma(f,z_p)e^{-4\alpha_S(f)(z_p)},$$
$$S(f,z_d) = P(f)D(f,z_d)\sigma(f,z_d)e^{-4\alpha_S(f)(z_d)},$$

where z_p and z_d stand for the depths of proximal window and distal window, respectively. $D(f,z_p)$ and $D(f,z_d)$ correct for the beam diffraction at the locations of the gated windows, $P(f)$ includes the frequency-dependent effects of the system acquisition and transducer, $\sigma(f,z_p)$ and $\sigma(f,z_d)$ correspond to the backscatter coefficients of the gated windows, and $\alpha_S(f)$ is the attenuation coefficient of the sample. Assuming a region with uniformly distributed scatterers spatially, $\sigma(f,z_p) \propto \sigma(f,z_d)$, then only the diffraction effects need to be compensated for estimation of $\alpha_S(f)$. For this purpose, additional backscattered signals are acquired from a well-characterized reference phantom using the same acquisition settings and transducer. The power spectra from two gated windows in the reference phantom located at the same axial positions as those used in the sample are

$$S_R(f,z_p) = P(f)D_R(f,z_p)\sigma_R(f,z_p)e^{-4\alpha_R(f)(z_p)},$$
$$S_R(f,z_d) = P(f)D_R(f,z_d)\sigma_R(f,z_d)e^{-4\alpha_R(f)(z_d)},$$

where the subscript R stands for the reference phantom. If the speed of sound of the reference phantom matches the speed of sound of the sample then $D(f,z_p) \approx D_R(f,z_p)$ and $D(f,z_d) \approx D_R(f,z_d)$. Therefore, the attenuation coefficient can be computed as

$$\alpha_S(f) = \alpha_R(f) + \frac{1}{4(z_d - z_p)} \log\left[\frac{S(f,z_p)S_R(f,z_d)}{S(f,z_d)S_R(f,z_p)}\right]. \quad (2)$$

A parameter derived from $\alpha_S(f)$ that is commonly used is the attenuation coefficient slope, i.e., the slope of the linear fit of $\alpha_S(f)$ with respect to $f \in (f_L, f_H)$, where f_L and f_H correspond to the lower and upper frequencies of an analysis frequency band around the center frequency of the transducer. This analysis band defines the band of frequencies of the power spectra involved in Eq. (2). In the present study, which used a source having a 5-MHz nominal center frequency, the analysis band ranged from 3.2 to 6.6 MHz in the numerical simulations and from 4.1 to 6.5 MHz in the

https://doi.org/10.1121/10.0001690

physical phantom studies. The lower bandwidth was used in the physical phantoms because of low signal-to-noise ratio in the experimentally acquired signals.

B. Computer simulation

In the present study, we quantified bias and variance of estimates of the attenuation coefficient due to the distortion caused by nonlinear acoustic propagation. In experiments with physical phantoms, the transducer behaves as a passband filter of the backscattered signals. Therefore, observation of nonlinear distortion through second harmonic generation in the backscattered signals is diminished because it is filtered in the passband operation. However, it is illustrative to use computer simulations with settings similar to those of the experiment to observe the second harmonic band generated without the aforementioned filtering effect. Nevertheless, computing the attenuation coefficient by Eq. (2) required only the fundamental frequency band around the excitation nominal frequency.

Computer simulated radio frequency (RF) data were generated with the k-Wave toolbox (Treeby *et al.*, 2012). Three numerical phantoms were used in the studies: one sample and two references (high and low attenuating), labeled S′, R_{HA}′, and R_{LA}′ to resemble the names of the physical phantoms (the prime superscript is used when referring to numerical simulated data) having the same attenuation and nonlinearity parameter as in Table I. Random spatial variations in the density (2% standard deviation) were defined generating media with spatially random impedance values such that backscattered signals mimicking those observed from physical phantoms could be generated. The simulated focused transducer acted as both a source and a receiver with a diameter of 0.5 in. and a 1 in. focal length and was configured in a three-dimensional (3D) grid such that a maximum frequency of 12.8 MHz was supported in the three axes using a spatial grid increments of 0.06 mm (this limitation of supported frequencies was set by the available computational resources). Figure 1 depicts the source/receiver used to simulate the data. k-Wave allowed the attenuation coefficient to be set with a uniform power-law attenuation coefficient across the medium with values from Table I. Likewise, in k-Wave it is possible to set a nonlinearity parameter B/A to include nonlinear distortion and generation of harmonics.

TABLE I. Speed of sound, attenuation coefficient, B/A, glass bead size ranges and concentrations of glass beads in physical phantoms: S (sample), R_{HA} (high attenuating reference), and R_{LA} (low attenuating reference).

	Phm. S	Phm. R_{HA}	Phm. R_{LA}
Speed of sound (mm/μs)	∼1.54	∼1.54	∼1.54
$\alpha(f)$ (dB/cm)	$0.27f^{1.32}$	$0.7f^{1.1}$	$0.028f^{1.75}$
B/A	6.8	6.9	6.0
Diameters (μm)	75 – 90	9 – 43	41 ± 2
Concentration	5/mm^3	800/mm^3	No info.

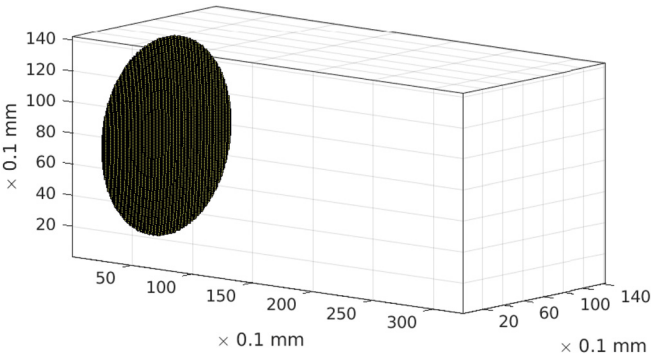

FIG. 1. (Color online) Source/sensor in numerical simulations depicted as a spherically focused geometry in discretized 3-D media. The focal length of 1 in. is smaller than the largest axial depth.

A limitation of k-Wave is that it cannot set arbitrarily small grid sizes without rapidly exceeding the computational resources, especially when the simulation was in 3D. To validate that our simulations were correctly capturing the nonlinear distortion in the fundamental band we used the Khokhlov–Zabolotskaya–Kuznetzov (KZK) model and its solver by Lee and Hamilton (1995) as the gold standard (because this software can generate several harmonics). We compared KZK waveforms to the waveforms generated in k-Wave. We simulated a forward broadband pulse propagation in a medium with square attenuation dependence on frequency (assumed by KZK model) with lower attenuation than the used phantoms, i.e., more likely to develop nonlinearities. The discrepancy between waveforms at the geometrical focus was less than 3.3% of the peak-to-peak pressure. Therefore, it was assumed that the k-Wave simulations at the chosen grid size correctly predicted the nonlinear behaviors in the phantoms.

A broadband pulse with a 5-MHz center frequency and 60% fractional bandwidth (–6 dB) was used as an input signal. The pulse was intended to mimic the waveform from the physical transducer, which was experimentally measured close to the transducer surface (4 mm from the surface) using a needle hydrophone (Precision Acoustics Ltd., Dorchester, UK). The normalized pressure and frequency components of this input signal are shown in Fig. 2. At 4 mm from the transducer surface, negligible nonlinear distortion of the pulse had occurred resulting in harmonics that were more than 20 dB below the fundamental frequency. The source was excited using three different source peak pressures: 340, 570, 870 kPa from the values used experimentally; and additionally two source peak pressures used solely in simulations: 1100 and 1330 kPa to assess the effects of nonlinear distortion over a range of pressures that might be encountered in practice. Echoes received at the sensor were recorded for each of the six source pressures. Fifteen independent RF lines for each random media were generated. Power spectra estimated from the independent realizations were ensemble averaged in order to smooth out the power spectra for the SLD method using the full 15 power spectra for the reference power spectrum and groups

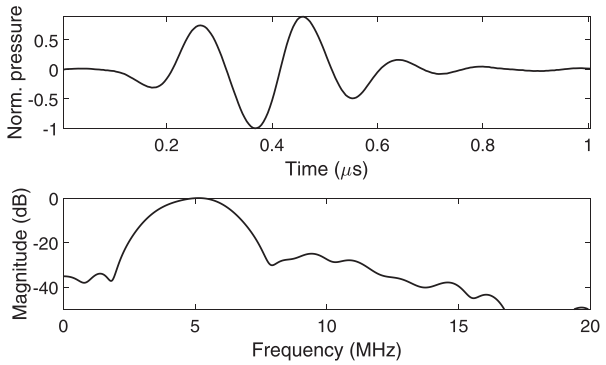

FIG. 2. Normalized pressure (top) and power spectrum (bottom) of the input excitation source used in the simulations. The time-domain waveform was chosen to mimic the waveform observed in the experiments when measured with a needle hydrophone at 4 mm from the surface of the transducer.

of five for the sample power spectrum, which provided three attenuation coefficient slope values per source pressure. Similar to the attenuation estimation used in the physical experiments, the attenuation coefficient of sample S′ was determined using the SLD method in two scenarios: (1) medium R_{HA}' (more attenuating) as the reference phantom and (2) medium R_{LA}' (less attenuating) as the reference phantom. The *B*/*A* values for the three simulated media were set to 6.8, 6.9 and 6.0 for numerical phantoms S′, R_{HA}' and R_{LA}', respectively, to match the *B*/*A* estimated for the corresponding physical phantoms. For calculation of the power spectra from the backscattered scan lines, the length of the gated windows were set at seven wavelengths, i.e., roughly two pulse lengths axially for both proximal and distal windows.

C. Experimental phantoms

For the physical phantom experiment, three agar-based tissue-mimicking phantoms containing glass bead scatterers were used and labeled S, R_{HA}, or R_{LA}. Physical phantoms of these types are often used to assess image quality performance of ultrasonic imaging techniques because the speckle features can be controlled by the glass bead concentration and attenuation by mixtures of bovine milk, agar, and degassed water. Each phantom had cylindrical shape with 3 in. diameter and 1.5 in. height and an agar-based matrix. The physical properties in Table I of the phantoms S and R_{HA} are described in Wear *et al.* (2005) as phantoms A and B; whereas the properties of phantom R_{LA} is described in the second column of Table I in Anderson *et al.* (2010).

Sound speeds were calculated using Eq. (4) in Wear *et al.* (2005), i.e., measuring arrival times of received broadband pulses with and without the sample in a water path. Ground truth attenuation coefficients of Table I were estimated using standard insertion loss methods (Kuc and Schwartz, 1979), i.e., immersing the phantoms in a water tank, accounting for mismatches between the speed of sound for water and the phantoms (Xu and Kaufman, 1993) and performing a least-square method to fit the attenuation coefficient to a power-law with respect to frequency (Madsen *et al.*, 1978) over the range from 2 to 7 MHz. To reduce the impact of nonlinear effects in determination of the ground truth attenuation coefficients both sound speed and attenuation were calculated with RF data acquired using a low power level pulser/receiver (5800PR, Panametrics Olympus, USA) in which the second harmonic signals recorded with a needle hydrophone for the water-only path were below 20 dB. The nonlinearity parameter, *B*/*A*, was estimated using the through-transmission method presented in Dong *et al.* (1999). Using this method, the estimated values of *B*/*A* for our phantoms (presented in Table I) were in agreement with results for phantoms of the similar type found in Dong *et al.* (1999). In order to compare attenuation coefficient slope estimates using the SLD technique against the ground truth estimates, it was necessary to estimate the slope values from the ground truth values of attenuation coefficient in Table I by fitting a straight line to the function over the analysis frequency band of 4.1 to 6.5 MHz. The ground truth attenuation coefficient slope values for phantoms S, $R_{HA,}$ and R_{LA} were 0.61, 0.91, and 0.17 dB/cm/MHz, respectively. For the simulations, because the analysis frequency range spanned from 3.2 to 6.6 MHz, the ground truth values were slightly different at 0.59, 0.9, and 0.16 dB/cm/MHz for S′, R_{HA}', and R_{LA}', respectively.

D. Ultrasonic scanning procedures

The attenuation coefficients were estimated from the phantoms using the SLD method at different source pressure levels to quantify the effects of the nonlinear distortion of the ultrasonic wave propagation on the accuracy of the attenuation coefficient estimates. Each phantom was immersed in a tank filled with degassed water and scanned using a single-element spherically focused transducer (ISR054, NdtXducer LLC, USA) having a 0.5 in. diameter and 1 in. focal length (see Fig. 3). The nominal frequency of the transducer was 5 MHz and was excited with a high-power pulsing apparatus (RAM-5000, Ritec, USA). The input signal applied to the transducer was a one-cycle sinusoidal at 5-MHz. Backscattered RF data were acquired by the same transducer for six excitation levels generated by the pulsing apparatus. The six excitation levels resulted in peak pressures of 340, 450, 570, 690, 780, and 870 kPa measured independently in water by a needle hydrophone at 4 mm from the transducer surface (see Fig. 2). The pressure levels of the signals from the transducer at each excitation level were also measured at the geometrical focus (see Table II) providing a strong nonlinear distortion as observed in Fig. 4.

Further power spectral smoothing occurred by averaging power spectra from RF data acquired by moving the transducer in a plane (grid of 14 mm × 14 mm) parallel to the surface of the transducer with 1 mm steps. This resulted in a backscattered power spectrum estimate from an ensemble average of 225 independent power spectra. The mean and standard deviation were calculated for three estimate values obtained at each excitation level by using a third (75

https://doi.org/10.1121/10.0001690

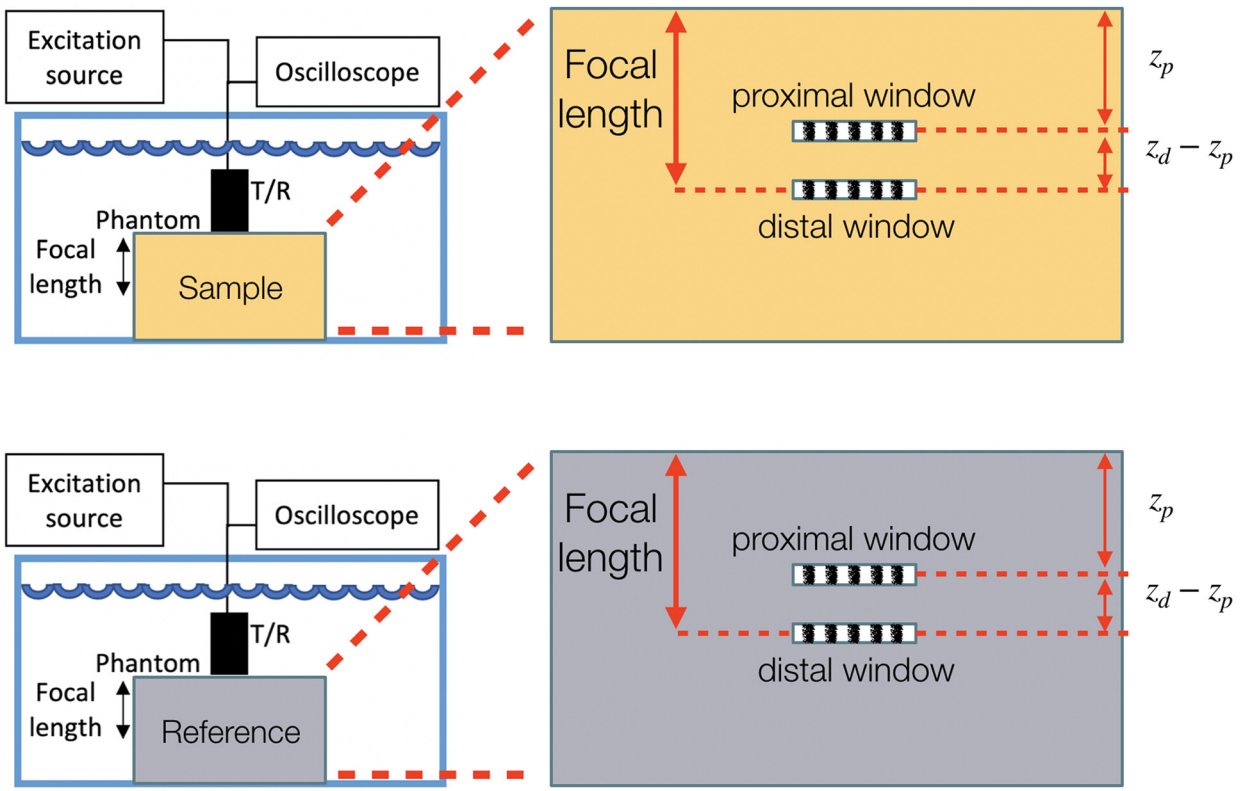

FIG. 3. (Color online) (Top) Depiction of the experimental setup when measuring from the sample and (bottom) depiction of the experimental setup when measuring from the reference phantom. Note that the experimental setup was the same between the sample and reference and only the sample was replaced with the reference phantom.

averaging of the 225 power spectra) of the sample power spectra. Nonlinear distortion of the ultrasound in the phantoms was expected to be less than in water because while the B/A is slightly lower in water than in the phantoms (e.g., B/A of 5 vs 6), the attenuation of water is more than an order of magnitude lower than the phantoms at 5 MHz.

Attenuation coefficient estimates were obtained for the phantom S, which was used as the sample, whereas phantoms R_{HA} and R_{LA} were used independently as references (high attenuating and low attenuating). In the estimation, the distal window was placed just after the focus (centered around 27 mm) and the proximal window 1 cm closer to the transducer. Phantoms S, R_{HA}, and R_{LA} had similar B/A values but different attenuation coefficient values. Reference phantom R_{HA} had higher attenuation than phantom R_{LA} suggesting that nonlinear distortion in the reference was more likely to develop in phantom R_{LA}. Once $\alpha_S(f)$ was obtained following Eq. (2), a linear fit was performed to obtain the attenuation coefficient slope (in dB/cm/MHz) and compared with the corresponding ground truth value derived using the $\alpha(f)$ from Table I. Finally the difference in the attenuation

TABLE II. Summary of peak positive pressure and peak negative pressure values associated with the settings used in the experiments, measured using a needle hydrophone at the geometrical focus $F = 1$ in. of the transducer. The mechanical index at the nominal frequency $f_0 = 5$ MHz was calculated using $\mathrm{MI} = \mathrm{PNP}\exp(-0.0345 f_0 F)/\sqrt{f_0}$ and found to be within the FDA regulated limits for diagnostic ultrasound ($\mathrm{MI} < 1.9$).

	Peak positive pressure (MPa)	Peak negative pressure (MPa)	MI
Excitation level 1	7.57	2.76	0.80
Excitation level 2	8.87	3.33	0.96
Excitation level 3	9.76	3.77	1.09
Excitation level 4	10.53	4.14	1.19
Excitation level 5	11.53	4.42	1.27
Excitation level 6	12.04	4.63	1.34

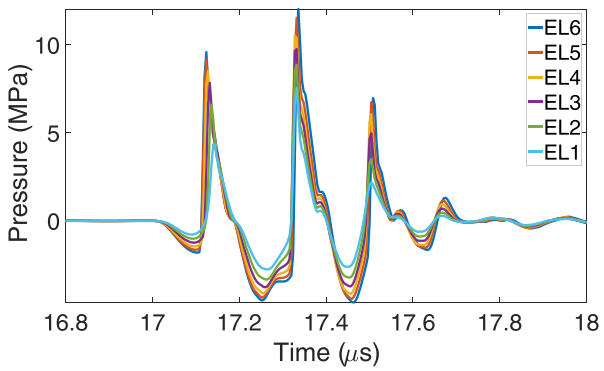

FIG. 4. (Color online) Waveforms measured at the geometrical focus of the transducer using a needle hydrophone when exciting the transducer with the six excitation levels (ELs). The nonlinear distortion is observable from the hydrophone measurements that were performed in water.

slope estimates between the lowest and highest excitation pressure levels was computed as

$$\Delta_{\text{slope}} = \text{slope}_{870kPa} - \text{slope}_{340kPa}. \quad (3)$$

III. RESULTS

A. Computer simulation

Figure 5 shows the power spectra from the numerical phantoms with proximal and distal windows for each excitation level used. The five different excitation peak pressures set in k-Wave at the source were 340 kPa (blue), 570 kPa (orange), 870 kPa (yellow), 1100 kPa (purple), and 1330 kPa (green). The numerical phantoms were simulated with nonlinearity parameters described in the Table I to mimic the acoustic properties of the physical phantoms.

In Fig. 5 the second harmonic components, roughly starting 8-MHz, can be observed because energy is transferred from the fundamental band to higher harmonics. From Fig. 5, the rate at which energy is transferred from the fundamental to harmonics depends on the source pressure level used and the acoustic properties of the phantoms such as the value of B/A and attenuation coefficient. Figures 6 and 7 provide estimates of the attenuation coefficient slopes for phantom S′ when using phantom R_{HA}' [Fig. 6(a)] as a reference and phantom R_{LA}' [Fig. 7(a)] as a reference. For example, when the more attenuating numerical phantom R_{HA}' was used as a reference, the attenuation coefficient slope of the sample varied from 0.66 ± 0.12 dB/cm/MHz for the smaller source pressure to 0.86 ± 0.13 dB/cm/MHz for the largest source pressure. The increase in the estimate of attenuation slope from the source pressure level 340 kPa to the source pressure level 870 kPa was Δ_{slope}=0.083 dB/cm/MHz. On the other hand, when the less attenuating numerical phantom R_{LA}' was used as a reference, the attenuation coefficient slope of the sample varied from 0.64 ± 0.13 dB/cm/MHz for the smaller source pressure to 0.43 ± 0.13 dB/cm/MHz for the largest source pressure. The decrease in the estimate of the attenuation slope from the source pressure level 340 kPa to the source pressure level 870 kPa was $\Delta_{\text{slope}} = -0.118$ dB/cm/MHz. Using either the high or low attenuating phantoms, at the lowest source pressure level the ground truth value 0.61 dB/cm/MHz remained within one standard deviation of the estimated mean value but larger bias is observed at the largest source pressure level.

The deviation in the estimates of the attenuation coefficient slope with increasing pressure indicated that nonlinear distortion could introduce changes in attenuation coefficient slope estimates with increasing source pressure. Furthermore, due to the attenuation of the different simulated phantoms, nonlinear

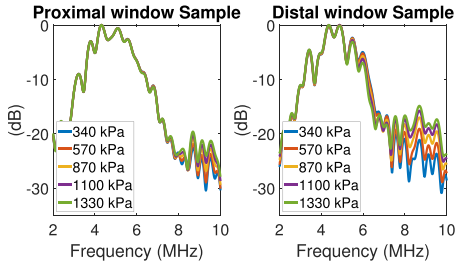

(a) Numerical phantom S′: $B/A = 6.8$ and $\alpha(f) = 0.27f^{1.32}\frac{\text{dB}}{\text{cm}}$

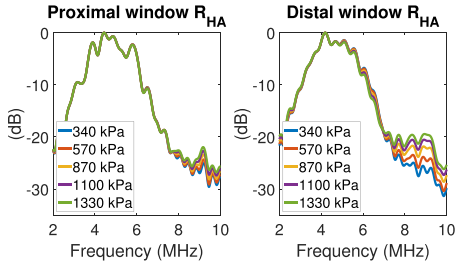

(b) Numerical phantom R_{HA}': $B/A = 6.9$ and $\alpha(f) = 0.7f^{1.1}\frac{\text{dB}}{\text{cm}}$

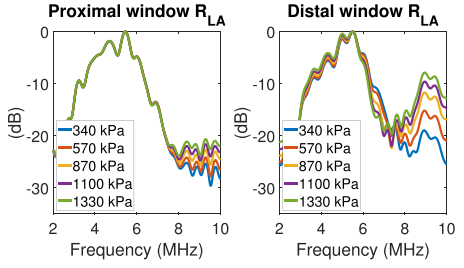

(c) Numerical phantom R_{LA}': $B/A = 6$ and $\alpha(f) = 0.028f^{1.75}\frac{\text{dB}}{\text{cm}}$

FIG. 5. (Color online) Power spectra from gated proximal and distal windows using five increasing source pressures in the numerical phantoms S′ (top), R_{HA}' (middle), and R_{LA}' (bottom). The proximal window was located before the geometrical focus and the distal window was located close to the geometrical focus. In computer simulations, larger levels of second harmonic are generated at the distal windows. Moreover, the low attenuating reference phantom (R_{LA}') power spectra had larger second harmonic generation for the larger acoustic pressures than S′ and R_{HA}'.

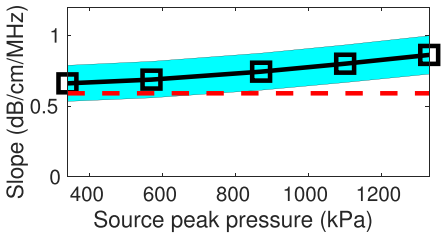

(a) Numerical phantom slope vs. source pressure

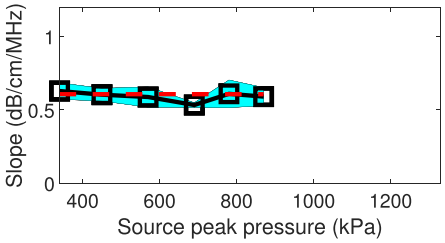

(b) Physical phantom slope vs. source pressure

FIG. 6. (Color online) Mean (square markers) of attenuation coefficient slope estimates of medium S for the numerical phantom (top) and physical phantom (bottom) when the reference was the high attenuating reference medium R_{HA}. Shadowed area corresponds to the standard deviation (one above and one below) of slope estimated mean values. The dashed red line was the ground truth slope.

https://doi.org/10.1121/10.0001690

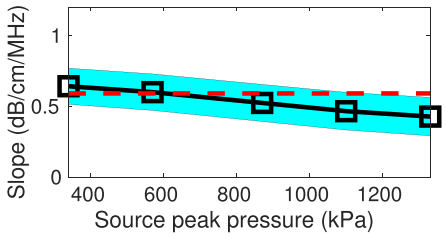

(a) Numerical phantom slope vs. source pressure

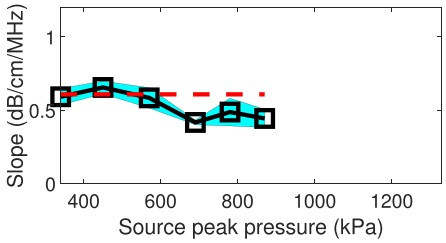

(b) Physical phantom slope vs. source pressure

FIG. 7. (Color online) Mean (square markers) of attenuation coefficient slope estimates of medium S for the numerical phantom (top) and physical phantom (bottom) when the reference was the low attenuating reference medium R_{LA}. Shadowed area corresponds to the standard deviation (one above and one below) of slope estimated mean values. The dashed red line was the ground truth slope.

distortion of power spectra from reference phantom R_{HA}' was slightly lower than for phantom S′ resulting in monotonically increasing estimates of attenuation coefficient slope and vice versa when using phantom R_{LA}' as the reference.

B. Experimental phantoms

The power spectra from proximal and distal regions used to estimate attenuation coefficient slope in the physical phantoms are presented in Fig. 8. In experiments, the second harmonic was mostly filtered out by the transducer. Similar to the power spectra in numerical phantoms, the fundamental band shifted to lower frequency especially at the distal window (closer to focus) with this shift more pronounced in the low attenuating phantom R_{LA}, Fig. 8(c), as pressure levels increased.

The attenuation coefficient slope values were estimated for phantom S and are shown in Figs. 6(b) and 7(b) when using phantoms R_{HA} and R_{LA} as references, respectively. Experimentally, it was observed that more consistent attenuation coefficient estimates were obtained when using references with higher attenuation coefficients, i.e., phantoms S and R_{HA}, in which case $\Delta_{slope} = -0.038$ dB/cm/MHz; whereas more inconsistency was observed when using phantom R_{LA} as the reference, i.e., $\Delta_{slope} = -0.148$ dB/cm/MHz. In the latter case, the ground truth value was outside of one standard deviation of the estimated slopes when using the largest source pressure level. However, unlike in the computer simulated phantoms, the values of the attenuation slopes did not change monotonically vs excitation level and the standard deviation were more variable across the excitation levels, which might be explained by lower signal-to-noise ratio of experimental backscattered data.

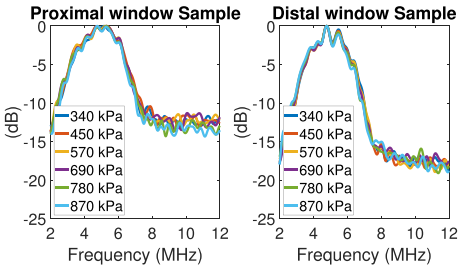

(a) Physical phantom S: $B/A = 6.8$ and $\alpha(f) = 0.27 f^{1.32}\,\frac{\mathrm{dB}}{\mathrm{cm}}$

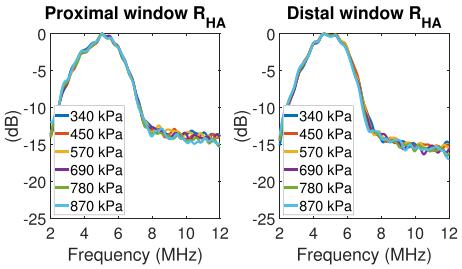

(b) Physical phantom R_{HA}: $B/A = 6.9$ and $\alpha(f) = 0.7 f^{1.1}\,\frac{\mathrm{dB}}{\mathrm{cm}}$

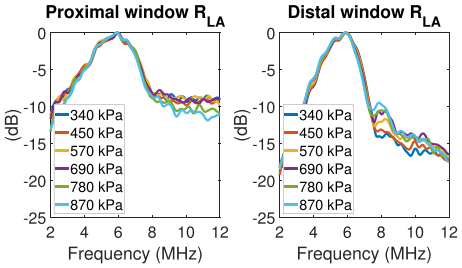

(c) Physical phantom R_{LA}: $B/A = 6.0$ and $\alpha(f) = 0.028 f^{1.75}\,\frac{\mathrm{dB}}{\mathrm{cm}}$

FIG. 8. (Color online) Power spectra from gated proximal and distal windows using six increasing source pressures in the physical phantoms S (top), R_{HA} (middle), and R_{LA} (bottom). The proximal window was located 1 cm before the geometrical focus and the distal window was located just after the geometrical focus. No second harmonic was clearly observable unlike the numerical simulations (Fig. 5) due to the filtering effect of the transducer.

IV. DISCUSSION

In the present study, we evaluated the SLD method for attenuation coefficient estimation when using increasingly higher acoustic pressures to assess if nonlinear distortion of ultrasound due to the nonlinearity of the medium would introduce biases in the attenuation coefficient estimates. We confirmed in numerical simulations, that second harmonic generation was likely to occur depending on several factors. The cases associated with the highest second harmonic generation included when larger input acoustic pressures at the source were applied, when the location of the gated window was closer to the geometrical focus, i.e., where larger pressures are expected due to focusing, and when less attenuating media were used that led to more rapid develop of nonlinear distortion.

The presence of nonlinear distortion can be quantified through the Gol'dberg number, which is proportional to the ratio of the nonlinearity coefficient and attenuation coefficient. In computer simulations we confirmed that both the

nonlinearity parameter and the acoustic attenuation of the medium affect the generation of the second harmonic. Moreover, the power spectra generated in the numerical simulations were consistent with the definition of Gol'dberg number. Therefore, acoustic nonlinearities result in energy in the fundamental band being transferred to higher harmonics (second harmonic presented in the numerical simulation). Thus, spectral methods for attenuation coefficient slope estimation that use the fundamental band produce biased attenuation coefficient estimates when non-negligible energy is transferred out of the fundamental band.

From the numerical simulations and experiments with physical phantoms we observed that attenuation coefficient estimates varied with different source pressures. These changes are associated with the nonlinear distortion of ultrasound in the sample and reference, which is observed in the power spectra at the fundamental band. Typically, distortions were observed to change more in the higher frequencies of the fundamental band than in the lower frequencies. This can be explained by the discontinuity distance descriptor $l = 1/\beta kM$ that suggests that generation of harmonics will occur over a shorter distance for higher frequencies components. In other words, higher frequencies are more rapidly transferred to higher harmonics resulting in a change in the slope over distance in the fundamental band of the backscattered power spectra in all cases. This distortion of the fundamental band is further enhanced in less attenuating media where the energy in the higher harmonics is not attenuated out as quickly resulting in more nonlinear distortion of the propagating pulse.

Although the Gol'dberg number is commonly defined for mono-frequency plane wave rather than a focused transducer, we utilized the Gol'dberg number to predict the presence of nonlinear distortion of the ultrasound. For the transducer geometry used in this study the Focal gain was $G = \pi a^2/\lambda F \approx 16.2$ (a is the radius of the source, $F = 1$ in. and λ the wavelength corresponding to the nominal frequency 5 MHz); therefore, the maximum Gol'dberg numbers, considering linear gain peak pressures at the focus, were between $\Gamma_S \in [8, 20.5]$, $\Gamma_{R_{HA}} \in [4.5, 11.4]$, and $\Gamma_{R_{LA}} \in [35.2, 90]$, over the source pressures range from 340 to 870 kPa. Therefore, a stronger second harmonic development in the lower attenuating numerical phantom R_{LA} was expected from the Gol'dberg number calculation and larger nonlinear distortion effects were predicted when using this phantom. It should be noted that because of nonlinear propagation effects, the actual linear focal gains, G, were not attained, i.e., positive peak pressure gains were larger than G whereas negative peak pressure gains were smaller than G (Bessonova *et al.*, 2009).

Similar results were observed when quantifying nonlinear distortion of ultrasound on the estimate of the backscatter coefficient (Coila and Oelze, 2019). In that study, the backscatter coefficient estimation process was analyzed using the reference phantom method and the traditional planar reflector technique in a water medium. The study found that a spectral-based method that used a nonlinear medium with low attenuation (i.e., water) produced large biases in the backscatter coefficient estimates. In that paper, the nonlinear distortion of ultrasound resulted in changes in the magnitude and slope of the backscatter coefficient because the references had different levels of nonlinear distortion. Specifically, using the water path for the reference resulted in much larger nonlinear distortion at high pressures when compared to using an attenuating reference phantom. Similar to attenuation coefficient estimation with the SLD, in the backscatter coefficient estimation, the sample and reference power spectra are used.

However, in the current work, the analysis was more complex, because up to four power spectra [see Eq. (2)] are involved in the estimation of the attenuation coefficient. One of the reasons for locating the distal window closer to the geometrical focus was to make the nonlinear distortion as large as possible whereas the nonlinear distortion in the proximal window located out of the focal region was not as strong. Therefore, the attenuation coefficient estimates depend mainly on $S(f, z_d)$ and $S_R(f, z_d)$. If the attenuation values of the sample and reference are known, we can predict whether the fundamental band will be distorted more in the sample or reference and predict a positive or negative bias in the attenuation coefficient estimates. For example, when the reference had lower attenuation than the sample, an apparent decrease in attenuation coefficients was observed. The opposite (increasing attenuation coefficients at higher excitation levels) occurred when the reference phantom had higher attenuation than the sample.

From the results in the numerical phantoms, the attenuation coefficient slope values obtained using the smallest pressure level and the largest pressure level had a mismatch that changed depending on the reference phantom used. This mismatch, Δ_{slope}, computed as in Eq. (3) can be correlated to the Gol'dberg number of the phantoms involved in the estimation (sample and reference) by comparing the results to the ratio of Gol'dberg number: $\Gamma_{Sample}/\Gamma_{Reference}$. From the acoustic properties of the phantoms described in Table I, at $f_0 = 5$ MHz, Gol'dberg number ratios for the different phantoms were $(\Gamma_{S'}/\Gamma_{R_{LA'}}) = 0.23$ and $\Gamma_{R_{HA'}}/\Gamma_{S'} = 0.56$. In addition, we calculated the attenuation coefficient slope of phantom R_{HA}' using the reference R_{LA}' resulting in an attenuation slope mismatch of $\Delta_{slope} = -0.20$ dB/cm/MHz with a Gol'dberg ratio of $\Gamma_{R_{HA'}}/\Gamma_{R_{LA'}} = 0.127$. Figure 9 shows the attenuation coefficient slope values at different pressure levels using the aforementioned pairs of samples/references where the increase or decrease of the Δ_{slope} depended on the ratio of Gol'dberg numbers.

Figure 10(a) shows a plot of values of Δ_{slope} vs Gol'dberg number while Fig. 10(b) shows a plot of the Δ_{slope} values vs the log of the Gol'dberg number ratios. Computing the coefficient of determination between Δ_{slope} vs $\log_{10}(\Gamma_{Sample}/\Gamma_{Reference})$ results in $R^2 = 0.979$. Similar calculation with the physical phantoms resulted in $R^2 = 0.734$. Empirically, one can observe that the mismatch of attenuation coefficient slope estimates from the different excitation levels due to acoustic nonlinearity is highly correlated to $\log_{10}(\Gamma_{Sample}/\Gamma_{Reference})$.

https://doi.org/10.1121/10.0001690

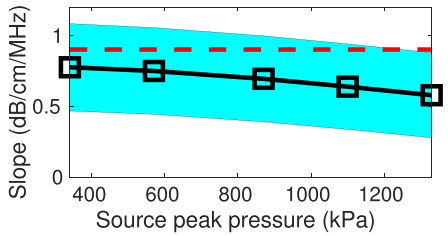

(a) Sample: R_{HA}. Reference: S

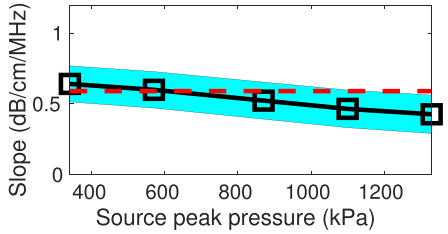

(b) Sample: S. Reference: R_{LA}

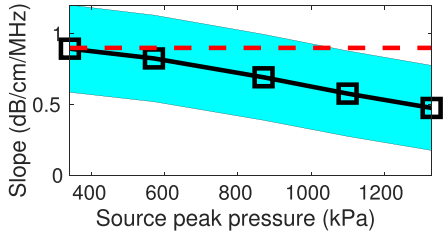

(c) Sample: R_{HA}. Reference: R_{LA}

FIG. 9. (Color online) Attenuation coefficient slope values vs source pressure level for three pairs of sample and reference. Large Gol'dberg ratios are correlated with increasing deviation of estimated attenuation slopes from baseline when using larger pressures.

V. CONCLUSION

In conclusion, the study findings suggest that attenuation coefficient estimation in pulse-echo mode using established methods, such as the SLD, can be biased due to the inherent acoustic properties of the sample medium and reference. The mismatch between the attenuation slope values from the true value during the ultrasonic acquisition of backscattered signals will increase when larger pressure levels are used. Moreover, the observed biases of attenuation coefficient slope estimates in both simulation and physical nonlinear media are more likely to occur in low attenuating media. Therefore, tradeoffs between the attenuation of the reference material, B/A, and need for strong signal-to-noise ratio should be considered when using methods like the SLD to estimate attenuation coefficients. After observing the pattern of increasing or decreasing attenuation coefficient slope estimates when using larger pressure levels, it was concluded that the attenuation values of the sample and reference should be close in order to reduce the effects of nonlinearity on the estimates and, therefore, the Gol'dberg number ratio between the sample and reference should be close to unity to mitigate nonlinear effects on attenuation slope estimation.

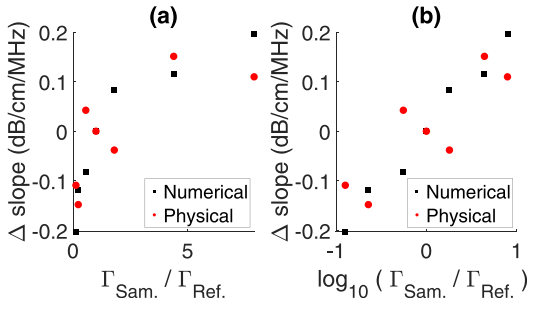

FIG. 10. (Color online) Mismatch of attenuation coefficient slope at low (340 kPa) and high (870 kPa) source pressures. Coefficient of determination was 0.754 vs $\Gamma_{Sample}/\Gamma_{Reference}$, and 0.979 vs $\log_{10}(\Gamma_{Sample}/\Gamma_{Reference})$ in numerical results. For the experimental data, the coefficient of determination was 0.564 vs $\Gamma_{Sample}/\Gamma_{Reference}$, and 0.734 vs $\log_{10}(\Gamma_{Sample}/\Gamma_{Reference})$.

ACKNOWLEDGMENTS

A.C. acknowledges the financial support from the National Council of Science, Technology and Technological Innovation (CONCYTEC, Perú) through the National Fund for Scientific, Technological Development and Technological Innovation (FONDECYT, Perú) under Grant No. 132-2016. The authors also acknowledge grants from the National Institutes of Health (NIH) (R21EB024133 and R21EB023403).

Anderson, J. J., Herd, M. T., King, M. R., Haak, A., Hafez, Z. T., Song, J., Oelze, M. L., Madsen, E. L., Zagzebski, J. A., O'Brien, W. D., and Hall, T. J. (**2010**). "Interlaboratory comparison of backscatter coefficient estimates for tissue-mimicking phantoms," Ultrasonic Imaging **32**(1), 48–64.

Bessonova, O. V., Khokhlova, V. A., Bailey, M. R., Canney, M. S., and Crum, L. A. (**2009**). "Focusing of high power ultrasound beams and limiting values of shock wave parameters," Acoust. Phys. **55**(4), 463–473.

Cobbold, R. S. C. (**2007**). *Foundations of Biomedical Ultrasound* (Oxford University Press, New York), p. 74.

Coila, A., and Oelze, M. L. (**2019**). "Effects of acoustic nonlinearities on the ultrasonic backscatter coefficient estimation," J. Acoust. Soc. Am. **146**(1), 85–94.

Deeba, F., Ma, M., Pesteie, M., Terry, J., Pugash, D., Hutcheon, J. A., Mayer, C., Salcudean, S., and Rohling, R. (**2019**). "Attenuation coefficient estimation of normal placentas," Ultrasound Med. Biol. **45**(5), 1081–1093.

Dong, F., Madsen, E. L., MacDonald, M. C., and Zagzebski, J. A. (**1999**). "Nonlinearity parameter for tissue-mimicking materials," Ultrasound Med. Biol. **25**(5), 831–838.

Fatemi, M., and Greenleaf, J. F. (**1996**). "Real-time assessment of the parameter of nonlinearity in tissue using 'nonlinear shadowing,'" Ultrasound Med. Biol. **22**(9), 1215–1228.

Jeon, S. K., Lee, J. M., Joo, I., Yoon, J. H., Lee, D. H., Lee, J. Y., and Han, J. K. (**2019**). "Prospective evaluation of hepatic steatosis using ultrasound attenuation imaging in patients with chronic liver disease with magnetic resonance imaging proton density fat fraction as the reference standard," Ultrasound Med. Biol. **45**(6), 1407–1416.

Kinsler, L. E., Frey, A. R., Coppens, A. B., and Sanders, J. V. (**2000**). *Fundamentals of Acoustics*, 4th ed. (Wiley, Hoboken, NJ), p. 483.

Kuc, R., and Schwartz, M. (**1979**). "Estimating the acoustic attenuation coefficient slope for liver from reflected ultrasound signals," IEEE Trans. Sonics Ultrason. **26**(5), 353–361.

Labyed, Y., and Bigelow, T. A. (**2011**). "A theoretical comparison of attenuation measurement techniques from backscattered ultrasound echoes," J. Acoust. Soc. Am. **129**(4), 2316–2324.

Lee, Y.-S., and Hamilton, M. F. (**1995**). "Time-domain modeling of pulsed finite-amplitude sound beams," J. Acoust. Soc. Am. **97**(2), 906–917.

Madsen, E. L., Zagzebski, J. A., Banjavie, R. A., and Jutila, R. E. (**1978**). "Tissue mimicking materials for ultrasound phantoms," Med. Phys. **5**(5), 391–394.

Mamou, J., and Oelze, M. L. (**2013**). *Quantitative Ultrasound in Soft Tissues* (Springer, New York).

Nasief, H. G., Rosado-Mendez, I. M., Zagzebski, J. A., and Hall, T. J. (**2019**). "A quantitative ultrasound-based multi-parameter classifier for breast masses," Ultrasound Med. Biol. **45**(7), 1603–1616.

Pierce, A. D. (**1989**). *Acoustics: An Introduction to Its Physical Principles and Applications* (Acoustical Society of America, Melville, NY), Chap. 11.

Treeby, B. E., Jaros, J., Rendell, A. P., and Cox, B. T. (**2012**). "Modeling nonlinear ultrasound propagation in heterogeneous media with power law absorption using a k-space pseudospectral method," J. Acoust. Soc. Am. **131**(6), 4324–4336.

Wear, K. A., Stiles, T. A., Frank, G. R., Madsen, E. L., Cheng, F., Feleppa, E. J., Hall, C. S., Kim, B., Lee, P., Jr., Brien, W. D. O., Oelze, M. L., Raju, B. I., Shung, K. K.,, Wilson, T. A., and Yuan, J. R. (**2005**). "Interlaboratory comparison of ultrasonic backscatter coefficient measurements from 2 to 9 MHz," J. Ultrasound Med. **24**(9), 1235–1250.

Weng, W. C., Lin, C. W., Shen, H. C., Chang, C. C., and Tsui, P. H. (**2019**). "Instantaneous frequency as a new approach for evaluating the clinical severity of Duchenne muscular dystrophy through ultrasound imaging," Ultrasonics **94**, 235–241.

Xu, W., and Kaufman, J. (**1993**). "Diffraction correction methods for insertion ultrasound attenuation estimation," IEEE Trans. Biomed. Eng. **40**(6), 563–570.